encit 2020

ABCM Associação Brasileira de Engenharia e Ciências Mecânicas

18th Brazilian Congress of Thermal Sciences and Engineering
November 16-20, 2020 (Online)

ENC-2020-0127
THERMODYNAMIC ANALYSIS OF A STIRLING CYCLE FOR SPACE POWER SYSTEMS

Ermerson Ferreira de Moura[1]
Guilherme Borges Ribeiro[2]
Izabela Batista Henriques[3]
Aeronautics Institute of Technology, São josé dos Campos, Brazil.
ermerson@ita.br[1], gbribeiro@ita.br[2], izabela@ita.br[3]

Abstract. *The great challenges currently for space exploration are energy generation and storage systems with high efficiency associated with low mass and compatibility, allowing missions with lower costs and launch risks. In dynamic power generation systems for space applications, the conversion cycle must have high reliability, low mass, and efficiency. The nuclear energy-associated Stirling cycle has these characteristics. For this, a thermodynamic model coupled with a heat pipe model was applied to analyze the energy efficiency of a free piston Stirling cycle for nuclear power generation in space. The model considered conduction losses (thermal bridge), heat pipe efficiency, finite and regeneration time. The compression ratio considerably influences the overall cycle efficiency, the temperature of the cold side influences the efficiency of the cycle more significantly than the hot source. The liquid metal has a great impact on the performance of the cycle. The use of sodium as a liquid metal for the dimensional parameters used in this paper reduces the efficiency of the cycle by 6.76% compared to the results obtained for lithium. The increase of the number of heat pipes has a greater impact on the efficiency of the machine than the individual increase in the dimensions of the pipe.*

Keywords: *Stirling Cycle, Nuclear Propulsion, Heat Pipes, Thermodynamic Analysis.*

1. INTRODUCTION

Great investment growth in the space sector is a trend for the coming years. Every day new countries are involved in these activities and we are entering a new era of history, in which the presence of humanity out of orbit is increasing and new planets are being explored. For space exploration missions in deep space as well as future planet colonization missions, and establishment of outposts on the moon becomes possible, more efficient energy generation systems are needed (Fan et al. 2017) (Fan et al. 2018). One of the necessary requirements for power generation systems in the space of high efficiency is to have high energy density, compactability, and low specific mass, as it reduces launch costs in order to make the mission viable (Fan et al. 2017). There are currently 3 possible energy sources that can be used for space applications: Chemical, solar and nuclear (Araujo and Guimarães. 2018). Chemical batteries still have several limitations for applications in deep space, and in inhospitable places, where the incidence of solar radiation is reduced photovoltaic systems become inefficient (Dai et al. 2020) (Fan et al. 2017). Nuclear power generation systems by fission is an alternative of high energy density, compactness, reliability, and long availability for long-term missions and has been attracting attention (Fan et al. 2018) (Dai et al. 2019) (Dai et al. 2020). The nuclear power generation systems combine high energy density and long life, which is necessary for long-term missions in deep space, for example, for interplanetary missions above 20kW, nuclear reactors provide the best electricity generation solution (Araujo and Guimarães. 2018).

Studies consider that nuclear power with electric propulsion (NEP) is an alternative that can allow space missions that extend the range of interplanetary exploration to colonization, with its viability dependent on the efficiency of the energy conversion cycle (Ribeiro et al. 2015) (Toubolian et al. 2014).

The energy that is provided through nuclear energy consists in the use of thermal energy from exothermic nuclear reactions, with radioisotope decay or nuclear fission being the most common mechanisms (Araujo and Guimarães. 2018). The nuclear power system mainly includes three subsystems: the reactor system, the energy conversion system and the heat rejection system (Fan et al. 2018). The extracted heat can be converted into useful electricity by applying static or dynamic conversion systems (El-Genk et al. 2008a).

Nuclear power generation systems can be classified as static (thermocouple converter, alkali metal thermoelectric converter and thermionic converter) and dynamic (Brayton, Stirling and Rankine engines). Static conversion systems do not use moving parts for power generation, which increases their reliability, however, their efficiency is reduced to less than 10% (Fan et al. 2017) (El-Genk 2008a) (El-genk et al. 2008b). Dynamic conversion systems have moving parts and

use the heat supplied by the reactor to produce mechanical work and convert it into electrical energy through an alternator. Dynamic systems like Brayton and Rankine cycle have an efficiency between 20% to 30% (Fan et al. 2017) (Ribeiro et al. 2015) (El-genk et al. 2008a).

The higher the efficiency of the conversion cycle, the better the thermal utilization and, consequently, the better kW / Kg ratio. Between the conversion cycles, the Stirling cycle has high efficiency, being one of the cycles that most closely matches the ideal Carnot machine, showing promise for energy conversion systems in space, due to its efficiency, good kW / Kg ratio, starting automatic, and reliability (Fan et al. 2017) (Campos et al. 2012) (Dai et al. 2020). A Stirling Cycle works basically in four thermodynamic processes: two isothermal and two isochoric processes (Fan et al. 2017) (Campos et al. 2012). All these processes are divided by isothermal compression, isochoric heating, isothermal expansion, isochoric cooling. The use of a free piston stirling cycle (FPSE) reduces the amount of moving parts, weight and the chances of failure, which increases the reliability of the conversion system (Fan et al. 2017).

In a standard nuclear energy conversion (FPSE) system the heat from the reactor is transferred by conduction to the evaporating section of the heat pipe; then, the heat moves to the condensing section through the flow of liquid metal into the heat pipe. (Dai et al. 2020) The heat provided by the condensing section of the heat pipe is transferred to the hot side of the FPSE by the heater connected to the heat pipe; subsequently, the cycle is carried out and the residual heat is rejected into the cooler section and rejected into space by heat pipes and radiator, radiation is the only way to reject heat into space (Fan et al. 2018). A typical FPSE mainly contains a heater, cooler, piston, displacer, expansion space, compression space, regenerator, pressure housing, support structure and linear alternators (Dai et al. 2020). The expansion space is connected to the heater and the compression space is connected to the cooler. The regenerator is a porous structure between the heater and the cooler; the regenerator provides a thermal barrier between the heat sources and is used to store energy during compression and then return it to the working fluid during expansion (Dai et al. 2020). The working gas used is Helium, due to its low viscosity, low density and high thermal conductivity to improve the performance of the Stirling cycle and decrease the resistance to flow within the FPSE. (Fan et al. 2017) (Dai et al. 2020).

The radiator and heat pipe assembly are responsible for the highest percentage of mass and dimensions in a typical system and may be the sole responsible for almost one third of the total mass of the conversion system (Juhasz. 2007), which indicates the importance of improving the heat rejection system. The focus of this work is to perform finite-time thermodynamic modeling for the stirling cycle, coupled with a one-dimensional heat pipe model for both the cold and hot sides, in order to increase the efficiency of the cycle, and power delivered per unit mass. Thus, it is possible to evaluate the effect of heat pipes with different dimensional parameters and to compare the impact on the overall efficiency of the heat pipes with different liquid metals. For this article, lithium and sodium will be compared. This work can provide insights and valuable theoretical support for Stirling Cycle analysis and design for nuclear power generation in space.

2. THERMODYNAMIC MODEL

For thermodynamic modeling, the following assumptions are made:

- The transfer of heat between the heat generated in the core to the heat pipe on the hot side occurs by conduction;
- Heat conduction leads to a heat loss between the hot side and the cold side of the Stirling cycle;
- The specific heat of the working fluid is constant;
- The working fluid is be modeled as an ideal gas;
- Regeneration in the regenerator is imperfect with uniform temperature distribution;
- The reactor is adiabatic, non-deformable, has no axis work and kinetic energy, an energy potential and shear work are neglected.

In figure 1, a schematic temperature-entropy diagram showing the heat transfer throughout the system is displayed.

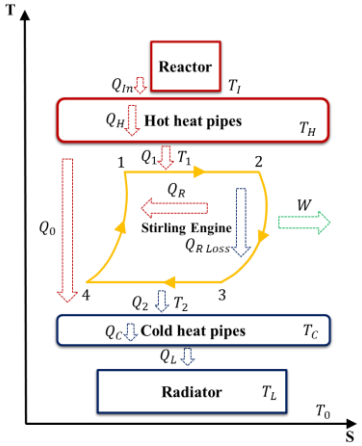

Figure 1. A schematic illustration of the various heat flows and losses adapted from Fan et al. (2017).

The heat that leaves the core and enters the heat pipe happens by means of thermal conduction, the fuel that supplies heat is on a rod made of zircaloy-2 usually with a thickness of 0.762mm according to The Nuclear Regulatory Commission. Considering heat transfer in a hollow cylinder and divided by the number of heat pipes and considering the same proportion of rods and heat pipes presented by Fan et al. (2017) it is defined:

$$\mathrm{Q_{in}} = -\frac{2\pi \mathrm{k_{rod}}(\mathrm{T_I} - \mathrm{T_0})}{\ln\left(\mathrm{r_2}/\mathrm{r_1}\right)\mathrm{N_{hp}}} \tag{1}$$

Where Q_{in}, are the heat transferred to the Stirling engine generated by the reactor, T_H is the heat pipe temperature; T_I core temperature, and r_1 is the fuel radius and r_2 is the radius rod; k_{rod} is the thermal conductivity of the rod; and N_{hp} is the numbers of heat pipes. The temperature T_H is the difference between the temperature of the core and the temperature step ΔT_{HP} of the heat pipe according equation (1):

$$\mathrm{T_H} = \mathrm{T_I} - \Delta \mathrm{T_{HP}} \tag{2}$$

This temperature step can be obtained by calculating the resistances associated with each section of the heat pipe. A conventional heat pipe is divided into three distinct regions: the evaporating region where the heat is added, the adiabatic, and condensing where the heat is rejected. The resistances considered for this model are: the resistance of the container, the wick region, the liquid-vapor interface, and the vapor region (Romano, 2018) (Reay et al. 2014). For the container can be described as:

$$UA_{con} = \frac{1}{2\pi K_{con} L_e} ln\left(D_{con}/D_{cap}\right) \tag{3}$$

Where K_{Con} the thermal conductivity of the casing material, Le the length of the evaporating region, D_{con} and D_{cap} are the diameters of the casing and the wick region. For the wick region, can be described as:

$$UA_{cap} = \frac{1}{2\pi K_{cap} L_e} ln\left(D_{cap}/D_{va}\right) \tag{4}$$

Where D_{va} the diameter of the steam region, and K_{cap}, described according to the following equation:

$$k_{cap} = \frac{\left(w_{fin}\, k_l\, k_{ti}\, d_{gr}\right) + w_{gr}\, k_l (0.185\, w_{fin}\, k_{ti} + d_{gr}\, k_l)}{\left(w_{gr} + w_{fin}\right)(0.185\, w_{fin}\, k_{ti} + d_{gr}\, k_l)} \tag{5}$$

Where w_{fin} the length of the wick groove, k_l is the conductivity of the working fluid, k_{ti} is the conductivity of the wall thickness of the wick region, d_{gr} is the deep groove, w_{gr} is the length of the wick groove. For the resistance of the liquid-vapor interface:

$$UA_i = \frac{R\, T_{va,e}{}^2 \sqrt{2\,\pi\, R\, T_{va}}}{MW\, 2\,\pi\, L_e\, h_{lv}{}^2} \tag{6}$$

Since R the gas constant, T_{va} the temperature of the vapor in the evaporator zone, MW is the molar mass of the fluid and h_{lv} the enthalpy of vaporization of the fluid in the evaporator region. For steam region, can be described as:

$$UA_{va} = \frac{\left(P_{va,e} - P_{va,c}\right)\left(\frac{\left(T_{va,c} + T_{va,e}\right)}{2}\right)}{h_{lv,va}\, \rho_{va}\, \dot{Q}_{hp}} \tag{7}$$

Where $P_{va,e}$ and $P_{va,c}$ the saturation pressure of the fluid in the evaporator and condenser region. T_{va} is the temperature of the vaporized fluid in the evaporating and condensing region. $H_{lv,va}$ the enthalpy of steam, ρ_{va} the density of the fluid and $\dot{Q}_{hp}$ the heat flux that enters the heat pipe. To Know UA_{hp} corresponding the overall thermal conductance of the heat pipe is used:

$$\frac{1}{UA_{hp}} = \frac{1}{UA_{con,e}} + \frac{1}{UA_{cap,e}} + \frac{1}{UA_{i,e}} + \frac{1}{UA_{va}} + \frac{1}{UA_{i,c}} + \frac{1}{UA_{cap,e}} + \frac{1}{UA_{con,c}} \tag{8}$$

Where the subscript “e “corresponds to the evaporating region and “c” for condensing region. In this way, the temperature step of the heat pipe is given by:

$$\frac{\mathrm{Q_{in}}}{\mathrm{UA}_{hp}} = \Delta \mathrm{T_{hp}} \tag{9}$$

For the heat pipe to operate normally, the values of diameters and lengths must be respected to reach limits of its operation, which are capillary, sonic, viscous, boiling, and entrainment limits. The limits were considered for each variation in the dimensions of the heat pipe as well as the maximum capillarity pressures. To validate the equations used and simplify the operation model of the heat pipe, the vapor flow rate of its working fluid is limited to a laminar and incompressible regime (Rev <2300 and Ma <0.2, respectively). For the Stirling engine the thermal bridge between the hot and cold side is proportional to the cycle time and is described by the following equation (Fan et al. 2017) (Feng et al. 2008):

$$\mathrm{Q_o} = \nu_0 \tau (\mathrm{T_H} - \mathrm{T_C}) \tag{10}$$

Where ν_o is the heat leak coefficient between the hot and cold side and T_C the cold side temperature. Regenerative heat transfer in the regenerator can be described as (Fan et al. 2017) (Feng et al. 2008):

$$\mathrm{Q_R} = \mathrm{nC_p}\varepsilon_\mathrm{R}(\mathrm{T_1} - \mathrm{T_2}) \tag{11}$$

Where n is the number of moles of the working fluid (Helium); C_p is the specific heat of the working fluid on a molar basis; ε_R is the efficiency of the regenerator, and T_1 and T_2 the temperatures of hot side and cold site of the regenerator. The heat loss Q_R in the regenerator can be described as follows (Fan et al. 2017)(Liao et al. 2015)(Ahmadi et al. 2013)(Yaqi et al. 2011):

$$\mathrm{Q_{R\,loss}} = \mathrm{nC_p}(1 - \varepsilon_\mathrm{R})(\mathrm{T_1} - \mathrm{T_2}) \tag{12}$$

The heat transfer that occurs between the hot and cold side heat exchangers to the working fluid takes place mainly by convection. The amount of heat absorbed by the working fluid on the hot side and released to the cold side can be described by the following equations (Fan et al. 2017)(Liao et al. 2015)(Ahmadi et al. 2013)(Yaqi et al. 2011):

$$\mathrm{Q_1} = \mathrm{UA_{HC}}(\mathrm{T_H} - \mathrm{T_1})\tau_1 = \mathrm{nRT_1 ln}\lambda + \mathrm{nC_p}(1 - \varepsilon_\mathrm{R})(\mathrm{T_1} - \mathrm{T_2}) \tag{13}$$

$$\mathrm{Q_2} = \mathrm{UA_{CC}}(\mathrm{T_2} - \mathrm{T_C})\tau_2 = \mathrm{nRT_2 ln}\lambda + \mathrm{nC_p}(1 - \varepsilon_\mathrm{R})(\mathrm{T_1} - \mathrm{T_2}) \tag{14}$$

Where Q_1 is the amount of heat absorbed by the working fluid; Q_2 is the amount of heat released by the working fluid; R is the universal gas constant; UA_{HC} is the convection heat transfer coefficient of the hot side heat exchanger and UA_{CC} is the convection heat transfer coefficient of the cold side heat exchanger; and λ is the compression ratio, being described as equation (15) (Fan et al. 2017):

$$\lambda = \frac{\mathrm{V_C}}{\mathrm{V_E}} \tag{15}$$

Where V_C is the volume of the compression side and V_E the volume of expansion side. The time of the processes τ_1 and τ_2 can be described as (Fan et al. 2017) (Liao et al. 2015)(Ahmadi et al. 2013)(Yaqi et al. 2011):

$$\tau_1 = \frac{nRT_1 ln\lambda + nC_p(1 - \varepsilon_R)(T_1 - T_2)}{UA_{HC}(T_H - T_1)} \tag{16}$$

$$\tau_2 = \frac{\mathrm{nRT_2 ln}\lambda + \mathrm{nC_p}(1 - \varepsilon_\mathrm{R})(\mathrm{T_1} - \mathrm{T_2})}{\mathrm{UA_{CC}}(\mathrm{T_2} - \mathrm{T_C})} \tag{17}$$

The time of the two isochoric processes τ_3 and τ_4 é described in equations (18) and (19) (Daim et al. 2018):

$$\tau_3 = \frac{\ln\left(1 - \left(1 + \frac{C_r}{C_f}\right)\frac{(T_1 - T_2)}{T_1 - T_C}\right)}{-\alpha_r\left(\frac{1}{c_r} + \frac{1}{c_f}\right)} \tag{18}$$

$$\tau_4 = \frac{\ln\left(1 - \left(1 + \frac{C_r}{C_f}\right)\frac{(T_1 - T_2)}{T_H - T_2}\right)}{-\alpha_r\left(\frac{1}{c_r} + \frac{1}{c_f}\right)} \tag{19}$$

Where C_r isochoric heat capacity of the regenerator, C_f isochoric heat capacity of the fluid being the ratio $C_f = m_r C_v$ where m_r is the mass fluid and c_v it the specfic heat of the fluid at constant volume; being $\alpha_r = h_r A_r$ where h_r is the heat transfer coefficient of the fluid and A_r the regenerator area. The total process time is the sum of the time of the four cycle steps, thus (Fan et al. 2017):

$$\tau = \tau_1 + \tau_2 + \tau_3 + \tau_4 \tag{20}$$

In a regenerator different speeds of the working fluid, and different conductivities in the regenerator results in non-uniform temperature distributions of the regenerator. For this model it will be assumed that the thermal conductivity of the regenerator is sufficiently large allowing the temperature distribution to be uniform. The heat transfer coefficient of the working fluid and the regenerator varies with time. According to (Daim et al. 2018) the efficiency of the regenerator can be defined as:

$$\mathrm{E_r} = \frac{(\mathrm{T_1} - \mathrm{T_C})}{\mathrm{T_H} - \mathrm{T_C}} = \frac{(\mathrm{T_H} - \mathrm{T_2})}{\mathrm{T_H} - \mathrm{T_C}} \tag{21}$$

With heat loss through thermal leakage the liquid heat absorbed and released by the heat exchanger can be described as follows:

$$\mathrm{Q_H} = \mathrm{Q_1} + \mathrm{Q_0} \tag{22}$$

$$\mathrm{Q_C} = \mathrm{Q_2} + \mathrm{Q_0} \tag{23}$$

Considering the cycle time of the Stirling engine, the system power (P) using the variables described above you could obtain (Fan et al. 2017)(Liao et al. 2015)(Ahmadi et al. 2013)(Yaqi et al. 2011):

$$P = \frac{\mathrm{W}}{\tau} = \frac{(\mathrm{Q_H} - \mathrm{Q_C})}{\tau} \tag{24}$$

Cycle energy efficiency (η_t) results in the following expression (Fan et al. 2017)(Liao et al. 2015)(Ahmadi et al. 2013)(Yaqi et al. 2011):

$$\eta_\mathrm{t} = \frac{(\mathrm{Q_H} - \mathrm{Q_C})}{\mathrm{Q_H}} \tag{25}$$

To determine the radiator area, the following is used (Incropera and Dewitt, 1990):

$$\mathrm{Q_{rad}} = \xi\sigma\mathrm{A_{rad}}(\mathrm{T_L^4} - \mathrm{T_0^4}) \tag{26}$$

Where ξ is the emissivity, σ the Stefan-Boltzmann constant, T_L is the temperature in the radiator panel. Merit figures relating the power delivered by the radiator area will be applied to obtain better cycle efficiencies According to Tarlecki (2007):

$$\psi = \frac{\mathrm{P}}{\mathrm{A_{rad}}} \tag{27}$$

3. RESULTS AND DISCUSSIONS

To verify the best characteristics for these system, the following parameters will be kept constant based on previous works: $D_{gr} = 0.5mm; w_{gr} = 5mm; w_{fin} = 0.5mm$; UACC=UAHC=200 W/K; n=1 mol; ε_R =0.8; σ=5.67.10-8 W/m²K^4 ; ξ=0.9; R=8.314 J/mol.K; ν0=2.5W/K; Cp=15 J/mol.K; λ=2;T_I=1200 K; K_{rod}= 21.5 W/m.K; $\alpha_r = 500$ W/m.K TC=300 K (Fan et al. 2017)(Romano et al. 2018)(Liao and Lin. 2015)(Ahmadi et al. 2013). The liquid metal in the heat pipe is lithium and the casing material is niobium. The behavior of sodium as a liquid metal was also evaluated in order to compare it with the results obtained with lithium. the temperature of the space in regions close to the earth can vary from

393 K to 100K, in this work a fixed temperature of 150 K was defined as the temperature of the environment. The number of heat pipes considered was 127 and 342 fuel rods according to the reactor presented by Fan et al. (2017). The diameter of the heat pipes considered was 12 mm and the lengths of the condensing and evaporating regions 0.5 m.

In order to verify the influence of the compression ratio in the stirling machine on the thermal efficiency of the system, the compression ratio was varied from 2 to 10 for different temperatures of the hot source as seen in the fig. 2. When comparing a compression ratio of 2 to 4 for a temperature of 700 K the difference in efficiency is 2.67% the difference is even greater when compared to a compression ratio of 8 where the difference in efficiency reaches 4%. The increase in the compression ratio on the Stirling machine considerably increases the overall efficiency of the system, however, from a compression ratio of 6 the increase in efficiency is negligible for lower temperatures and for higher temperatures a small increase. For a temperature of 1400K and a compression ratio of 8 the efficiency of the machine is 46.12% while with the compression ratio of 10 the efficiency achieved is 46.53%, a difference of 0.41%. Considering the considerable increase in mass of the stirling machine to increase the compression rate, compression rates above 6 do not show considerable benefits for the temperatures and parameters considered in this model.

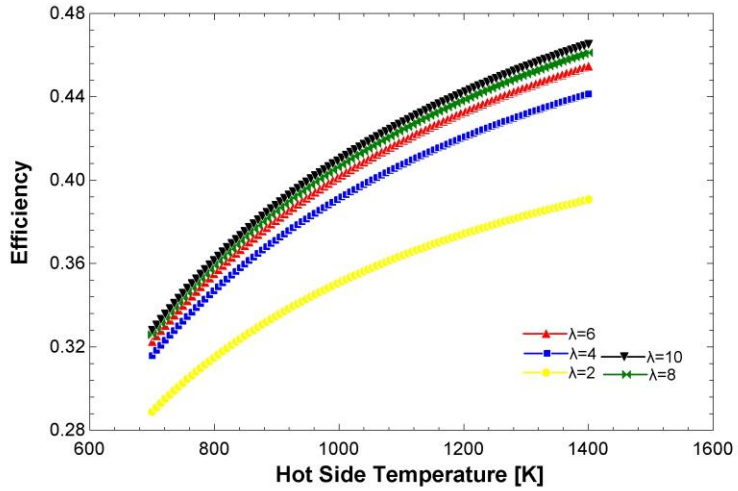

Figure 2. Energy efficiency by the hot side temperature.

In figure (3) the efficiency of the cycle was evaluated for differences compression ratios and cold source temperatures. With lower temperatures and a compression ratio of 10 it was possible to obtain a machine efficiency of 48.71% for the same temperature with a compression ratio of 2 the efficiency found is 40.6%, a difference of 8.11%. With the increase in temperature, the efficiency of the machine has a significant drop. For the temperature of 600 K, the efficiency of the machine reaches 22.22% for a compression ratio of 2, a difference of 18.38% compared to a temperature of 200 K. A considerable efficiency increase is evidenced when the ratio is increased from 2 to 6, but an increase higher than this does not have a very significant gain in efficiency. For a compression ratio of 6 and a cold side temperature of 200 K, the machine has an efficiency of 47.55%, and for a ratio of 8 an efficiency of 48.27% is found, a difference of 0.72%. The increase of temperature on the cold side has a greater impact on efficiency than the reduction of temperature on the hot side, which indicates the importance of a robust heat rejection system for a more efficient machine.

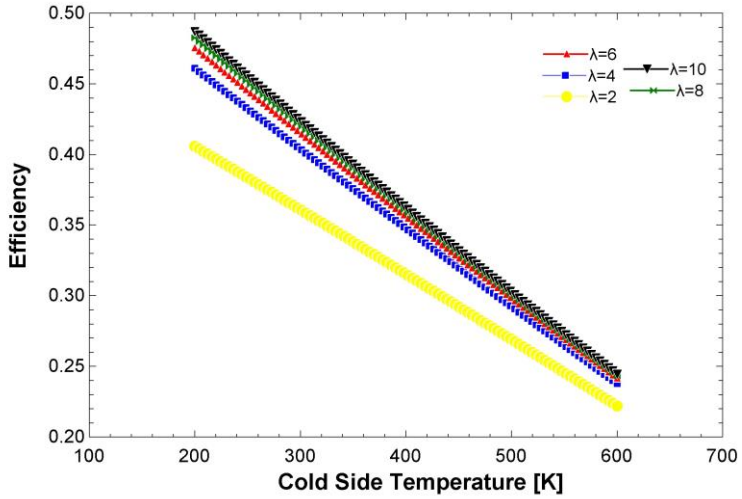

Figure 3. Energy efficiency by the cold side temperature.

The result of figure 3 indicated the importance of a proper heat rejection system for the efficiency of a Stirling achine. As the machine presented in this work is tailored for space applications, heat rejection occurs exclusively through radiation. Thus, to achieved a good heat rejection, the radiator and heat pipe assembly must have larger dimensions, influencing the overall size and mass of the power system. In figure 4 the figure of merit ψ that relates the power of the machine by area of the radiator was used to evaluate the influence of the size of the radiator and the power delivered. The highest W / m² ratio was found for temperature 676.8 K, presenting 2639 W / m². However, only a power of 1.7 KW is provided, with a panel area of 0.6585 m² and a efficiency of 18.57%. As the temperature of the cold side of the Stirling engine depends on the radiator, being a radiator with a small area (0.6585 m²), the temperature of the cold side becomes high which reduced the temperature difference between the cold side and the hot side , decreasing cycle efficiency and the power output. as it is a very small radiator area, the ψ has reached a high value. For a temperature of 200 K, the machine reached a ratio of 91.89 W / m² and a power of 9.7 KW. However, the radiator area was 106 m², increasing the dimensions and mass of the radiator. On the other hand, with the increase in temperature (1000 K) the machine presented a ratio of 211.6 W / m² with a radiator area of 0.1607 m², but presented a very small power and efficiency, 34W and 2.74%, respectively. Therefore, this figure of merit is a good indicator for optimal values of W / m². However, one must take into account the design power for a better dimensioning of the machine, aiming a lightweight conversion system with good efficiency.

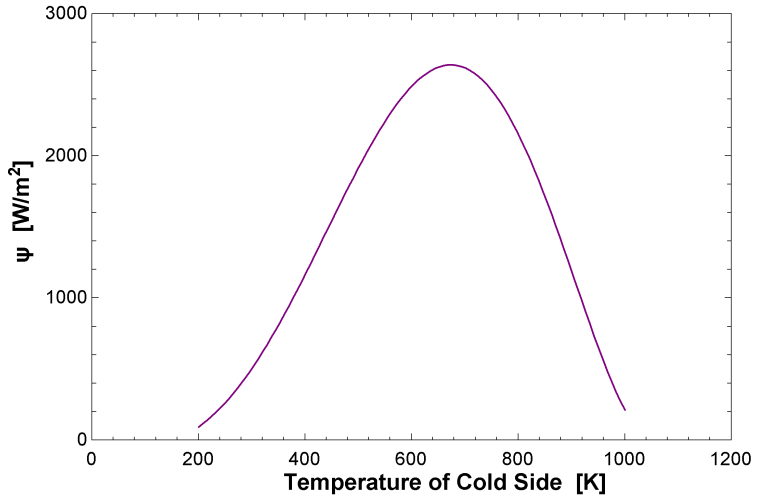

Figure 4. Figure of merit by the cold source temperature

The reactor heat pipes play an important role in delivering heat to the Stirling machine. Higher efficiency heat pipes will have a lower temperature drop and, therefore, it will be possible to obtain higher T_H temperatures which will influence the efficiency of the cycle. In figure 5 the efficiency of the machine was compared with the influence on the length of the region and evaporating and condensing of the heat pipes.

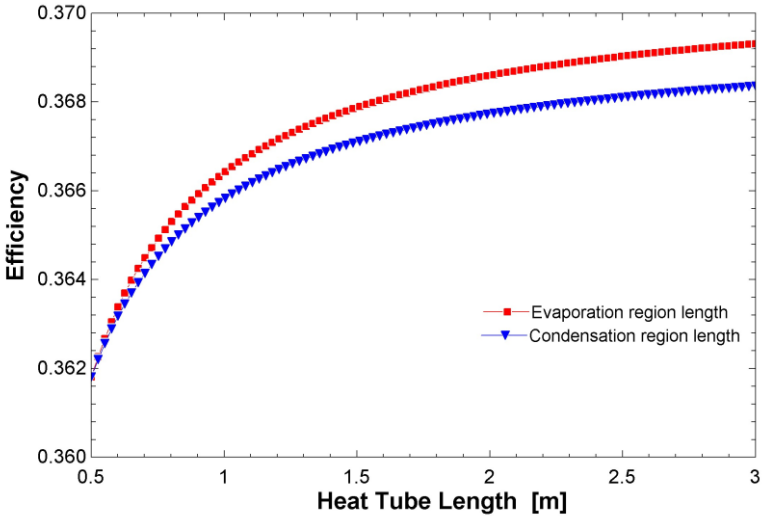

Figure 5. Energy efficiency by the heat pipe length.

The increase in the evaporating region has a greater influence on the machine efficiency than the increase in the condensing region. With the increase in the length of the heat pipe from 0.5 m to 3 m there was an increase from 36.09% to 36.93% an increase of 0.84%. With the increase in the condenser region, the enhancement was 0.75%. The increase is relatively low for a large increase on the dimensions of the heat pipes. When 127 pipes are considered, a negative influence on the system mass is expected. In Figure 6 the diameter of the heat pipe was varied to verify the impact on the efficiency of the Stirling engine. With the increase in diameter from 12 mm to 20 cm, an increase from 36.09 to 36.19% was found. Thus, it is not advantageous to increase the diameter of the pipes to increase the power system efficiency, especially when the mass increase is taken into account. An increase in the diameter of the heat pipe from 12 mm to 30 mm causes a greater relative increase in the thermal efficiency of the cycle, than the increase obtained when increasing the diameter to dimensions greater than 30 mm.

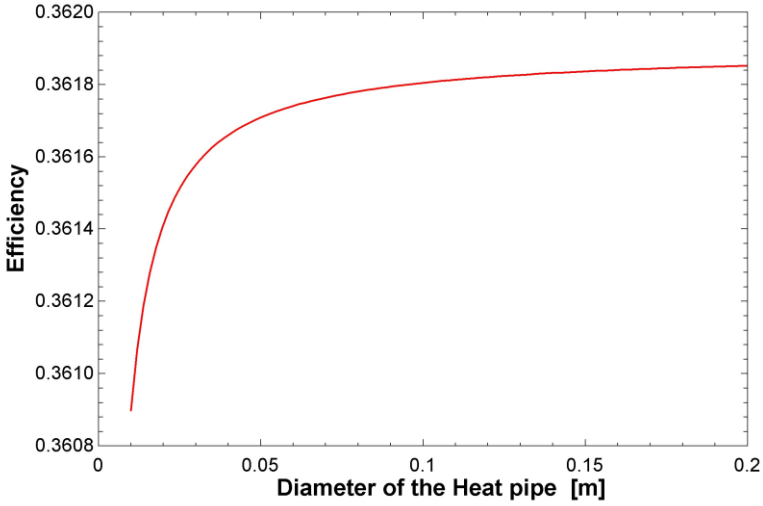

Figure 6. Energy efficiency by the heat pipe diameter.

In order to verify the effect of the heat pipe working fluid on the efficiency of the Stirling cycle, liquid lithium was replaced by sodium. Figure 7a. compares the effect of the length of the heat pipe on the overall efficiency of the cycle. For the 0.5 m length, the sodium heat pipe showed an efficiency of 29.33%, that is 6.76% less than for lithium, considering the same diameter and length. Again, a greater impact on the efficiency increase is found in the evaporating region. The increase in pipe length had a greater impact on the efficiency of the machine when sodium is used as the working fluid in the heat pipe. There is a 4.9% increase in efficiency when the length of the evaporating region is increased from 0.5 m to 3 m. However, the efficiency of the power system is still low in comparison with the lithium pipes. In figure 7b. the effect of increasing the diameter of the sodium heat pipe on efficiency is evaluated. With an increase in diameter from 12 mm to 20 cm, a 0.14% increase in efficiency is observed. This result indicates that the increase in diameter of the sodium heat pipes for the parameters used in this paper is not feasible. The sodium heat pipe showed the same behavior as the lithium heat pipe when the diameter from 12 mm to 30 mm is increased.

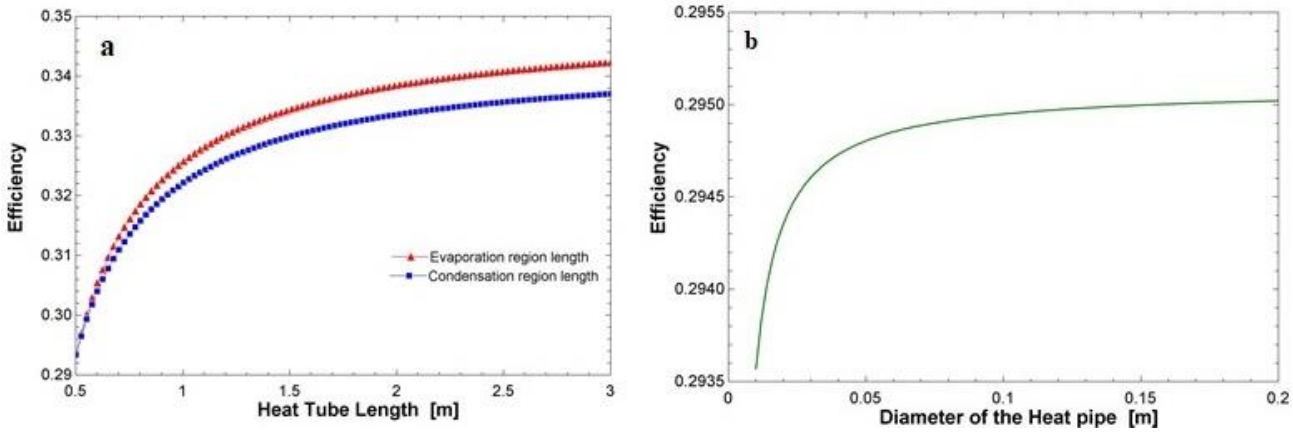

Figure 7. (a) Energy efficiency by sodium heat pipe length. (b) Energy efficiency by the sodium heat pipe diameter.

In figure 8a. the influence of the increase in lithium heat pipes on the efficiency of the cycle was verified considering a diameter of 12 mm and a length of 0.5 m for the evaporating and condensing region. With the increase from 127 pipes to 527 there was a 1.3% increase in the efficiency of the machine. The temperature drop decreases from 145.6 K to 35.32 K, a difference of 110.28 K. Thus, an increase in the number of pipes have a more positive impact than the individual increase in the dimensions of the pipes. In figure 8b. the influence of the increase in Sodium heat pipes on the efficiency of the cycle was verified. An increase in the quantity of sodium heat pipes from 127 to 527 provided an increase of 7.05%, a much larger percentage increase than that obtained with lithium pipes. However, even with 527 sodium heat pipes, the cycle is less efficient than that obtained with 127 lithium heat pipes.

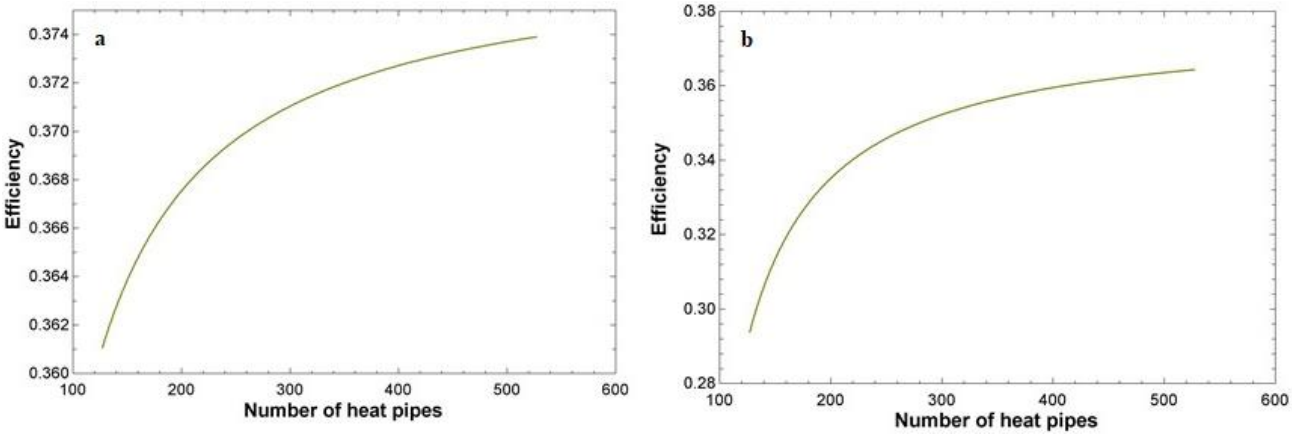

Figure 8. (a) Energy efficiency by Lithium Heat pipe. (b) Energy efficiency by Sodium Heat pipe.

The figure of merit ψ for the temperature of the cold side was evaluated considering sodium heat pipes, as shown in fig. 9. With a temperature of 454.3 K the highest value of ψ was obtained being 529.6 W / m² and presenting a radiator area of 2.202 m², power of 1.16 KW and efficiency of 18.57%. The cycle using sodium heat pipes showed a figure of merit 3 times lower than that obtained with lithium heat pipes. As the temperature drop of the sodium heat pipes is higher than that of the lithium heat pipes, the temperature of the hot side becomes lower, decreasing the overall efficiency of the system, affecting the power of the stirling engine and consequently the figure of merit ψ.

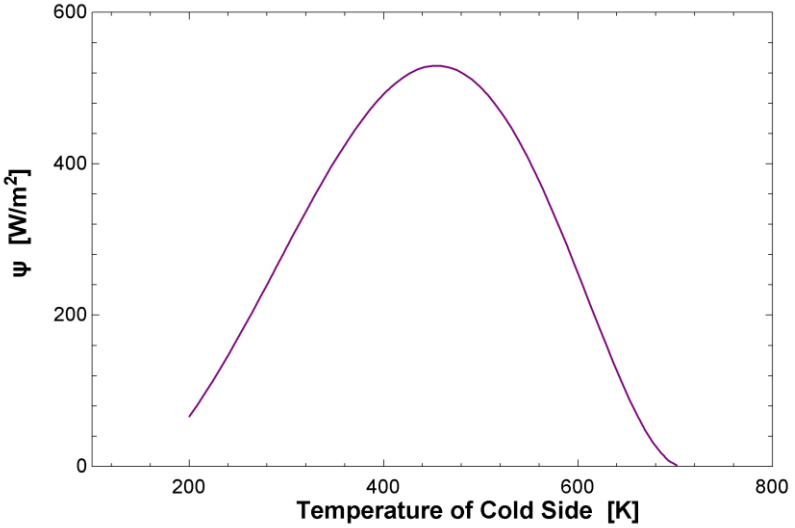

Figure 9. Figure of merit by the cold source temperature for Sodium heat pipe.

4. CONCLUSION

In the present work, thermodynamic analysis was applied to a power cycle of Stirling nuclear power generation in space. From the developed model, it was possible to identify that the compression ratio has the potential to significantly influence the efficiency of the system. The cold side temperature has the potential to reduce or increase machine efficiency more significantly than the hot side temperature, which reinforces the importance of a proper rejection system. The Stirling cycle with lithium heat pipes has a maximum ratio of ψ for the temperature of 676.8 K presenting 2639 W / m². However, this configuration presents only a power of 1.7 KW.

Regarding the heat pipes, it was verified that the increase in the length and diameter of the heat pipes for the parameters used in this work did not have a significant impact on system efficiency. With the use of sodium as a working fluid in the heat pipes, there is a considerable reduction in cycle efficiency compared to lithium heat pipes, even for smaller heat pipe dimensions. The Stirling cycle with sodium heat pipes with a length of 3 meters or a diameter of 20 cm has a lower thermal efficiency than with lithium heat pipes with a diameter of 12 mm and a length of 0.5 m. The increase in the number of heat pipes of sodium or lithium has a greater impact on reducing the temperature drop and increasing efficiency than the increase in efficiency achieved by changing heat pipe dimensions.

5. REFERENCES

Araújo EF, Guimarães LNF *"American Space Nuclear Electric Systems"*. J Aerosp Technol Manag. (2018) 10:e4418.

Ahmadi M.H, Sayyaadi H., Dehghani S., Hosseinzade H. *"Designing a solar powered Stirling heat engine based on multiple criteria: maximized thermal efficiency and power"*. Energy Convers. Manage 75 (2013) 282–291.

Campos, M.C., Vargas, J.C. *"Ordonez, Thermodynamic optimization of a Stirling engine"*. Energy 44 (2012) 902–910.

Dai D.D, Yuan F., Long R., Liu Z.C., Liu W. *"Imperfect regeneration analysis of Stirling engine caused by temperature differences in regenerator"*. Energy Conversion and Management 158 (2018) 60–69

Dai Z., Wang C., Zhang D., Tian W., Qiu S., Su G.H. *"Design and analysis of a free-piston stirling engine for space nuclear power reactor"*. *Nuclear Engineering and Technology* (2020),

Dai, Z., Wang, C., Zhang, D., Tian, W., Qiu, S., Su, G.H. *"Thermoelectric characteristics analysis of thermionic space nuclear power reactor"*. International journal of energy research, 2019, vol 4.

El-Genk, M.S. *"Space nuclear reactor power system concepts with static and dynamic energy conversion"*. Energy Conversion and Management, v. 49, n. 3, p. 402–411, 2008a.

El-Genk, M.S. *"Space reactor power systems with no single point failures"***.** Nucl.Eng. Des. 238 (2008b) 2245–2255.

Fan S. , Hu, Y., Li M. , Li S. , Zhou T. *"Thermodynamic performance of lunar surface nuclear power system with heat sink temperature change in a rotational period"*. Applied Thermal Engineering 130 (2018) 127–134

Fan S.,LI M., LI S., Zhou T., Hu Y., Wu S. *"Thermodynamic analysis and optimization of a stirling cycke for lunar surface nuclear power system"*. Applied Thermal Engineering 111 (2017) 60-67.

Feng W., Lingen C., Fengrui S., Jiuyang Y. *"Performance Optimization of Stirling Engine and Cooler Based on Finite-Time Thermodynamic"*. Chemical Industry Press, Beijing, 2008.

Incropera, F.P.; Dewitt, D.P. Fundamentals of Heat and Mass Transfer, 3a ed. LTC. S. A., R. J. 1990. P 74, P. 526.

Juhasz, A. "*Heat Transfer Analysis of a Closed Brayton Cycle Space Radiator"*. 5th International Energy Conversion Engineering Conference and Exhibit (IECEC), n. June, p. 25–27, 2007.

Liao T., Lin J. *"Optimum performance characteristics of a solar-driven Stirling heat engine system"*. Energy Convers. Manage 97 (2015) 20–25.

Reay D. A., Kew P. A., Mcglen R. J. *"Heat pipes"*. 6th. ed. Amsterdam: Elsevier, 2014.

Ribeiro G.B, Filho F.A.B., Guimarães L.N.F. *"Thermodynamic analysis and optimization of a closed regenerative Brayton cycle for nuclear space power systems"*. Appl. Therm. Eng. 90 (2015) 250–257.

Romano, Luis F. R. "*Thermal study of a heat pipe-radiator assembly for nuclear space power systems"*.161p. Master's dissertation – Aeronautics Institute of Technology, São José dos Campos, 2018.

Tarlecki J., Lior N., Zhang N. "*Analysis of thermal cycles and working fluids for power generation in space."* Energy Convers. Manag. 48 (2007) 2864 e 2878.

The Nuclear Regulatory Commission. "*General Electric Systems Technology Manual*" Available in: < https://www.nrc.gov/docs/ML1125/ML11258A302.pdf> Access: 24/09/2020

Tomboulian, B. N. *"Lightweight, High-temperature radiator for in-space nuclear-electric power and propulsion"***.** 2014. 205p. Theses (PhD) - Mechanical and Industrial Engineering Department, University Massachussets Amherst, Amherst.

Yaqi L., Yaling H., Weiwei H. *"Optimization of solar-powered Stirling heat engine with finite-time thermodynamics"*. Renew. Energy 36 (2011) 421–427.

6. RESPONSIBILITY NOTICE

The Authors are the only responsible for the printed material included in this paper.